Available online at www.sciencedirect.com
SCIENCE DIRECT®
Journal of Solid State Chemistry 177 (2004) 1268–1275
JOURNAL OF SOLID STATE CHEMISTRY
http://elsevier.com/locate/jssc

Structural evolution of Pt/ceria–zirconia TWC catalysts during the oxidation of carbon monoxide

A. Martorana,[a,b,*] G. Deganello,[a,b] A. Longo,[b] A. Prestianni,[a] L. Liotta,[b] A. Macaluso,[a] G. Pantaleo,[b] A. Balerna,[c] and S. Mobilio[c,d]

[a] *Dipartimento di Chimica Inorganica e Analitica "Stanislao Cannizzaro", Università di Palermo, viale delle Scienze, 1-90128 Palermo, Italy*
[b] *ISMN-CNR, Sezione di Palermo, via Ugo La Malfa 153, 90146 Palermo, Italy*
[c] *INFN-LNF, via Enrico Fermi 44, 00044 Frascati, Italy*
[d] *Dipartimento di Fisica "E. Amaldi", Università di Roma Tre, via della Vasca Navale 84, 00146 Roma, Italy*

Received 18 July 2003; received in revised form 27 October 2003; accepted 5 November 2003

Abstract

The structural evolution of two Pt/ceria–zirconia catalysts, characterized by different amounts of supported Pt, was monitored by in situ X-ray diffraction during the anaerobic oxidation of CO at different temperatures. In a first phase, oxygen coming from the surface layers of the ceria–zirconia mixed oxide is consumed and no structural variation of the support is observed. After this induction time, bulk reduction of Pt/ceria–zirconia takes place as a step-like process, while the CO_2 production continues at a nearly constant rate. This behavior is totally different from that of the metal-free support in similar reaction conditions, that show a gradual bulk reduction. In repeated oxidation–reduction cycles, it was observed that the induction time in Pt/ceria–zirconia is a function of the thermal history, of the amount of supported Pt and of the structural evolution of the samples.

Keywords: In situ XRD; synchrotron radiation; TWC; Ceria–zirconia; CO oxidation

1. Introduction

Three-way catalysts (TWC) are constituted of a metal nanophase supported on modified CeO_2. Due to the peculiarity of ceria that acts as an oxygen buffer, the TWCs are employed for the exhaust treatment in gasoline-fuel vehicles to achieve simultaneous control of CO, hydrocarbons and NO emissions [1]. TWCs constituted of platinum supported on ceria–zirconia solid solution show enhanced oxygen-storage properties with respect to ceria alone [2] and are extensively investigated. The oxygen-storage capacity of ceria is based on the redox process of the Ce(IV)/Ce(III) couple, involving oxygen take up from lean fuel gas and oxygen delivery during fuel-rich conditions [1]. This property allows to control the reaction environment that can be kept within a narrow composition range in order to ensure the effective catalytic removal of all the pollutants. Platinum promotes the NO conversion [3], as well as the oxidation of CO and hydrocarbons [4].

Most of the recent research on TWCs is devoted to the development of new systems that should comply with the zero emission demand of the forthcoming international rules. With this aim, it is important to improve the catalytic performance at the relatively low temperatures (473–573 K) of cold-engine regime that produces the maximum environmental pollution. A remarkable property of Pt/ceria and Pt/ceria–zirconia catalysts is their enhanced activity with respect to ceria alone in the cold-engine regime [5–6], although the relation activity-structural modification, in different reaction environments, is not yet clear. Therefore, a thorough structural characterization of TWC systems during various treatments could be very important for the development of better catalysts.

The different ionic radii of Ce(IV) (0.97 Å) and Ce(III) (1.14 Å) produce, in reductive or oxidizing environment, a variation of the lattice constant of ceria-based promoters that can be monitored by in situ X-ray diffraction (XRD) [7]. The use of in situ XRD for

*Corresponding author. Fax: +1-39-091-6809399.
E-mail address: cric2@unipa.it (A. Martorana).

0022-4596/$ - see front matter © 2003 Elsevier Inc. All rights reserved.
doi:10.1016/j.jssc.2003.11.001

the structural analysis of TWC systems was for the first time exploited by Ozawa et al. [8] and recently by Rodriguez et al. [9]. This paper reports on the structural modifications of two Pt/ceria–zirconia catalysts, 0.5 and 1 Pt wt%, respectively, in different conditions of flowing gas mixtures and of isothermal treatment temperatures; this behavior is compared with that of a metal-free ceria–zirconia sample.

2. Experimental

2.1. Sample preparation

The synthesis of ceria–zirconia mixed oxide with nominal composition $Ce_{0.6}Zr_{0.4}O_2$ was accomplished by using a sol–gel procedure that provides pure, reproducible, homogeneous and high thermally resistant materials [10]. Calculated amount of $Zr(OCH_2CH_2CH_3)_4$ (70% in *n*-propanol, Aldrich) was added to $Ce(NO)_3 \cdot 6H_2O$ (99.999%, Aldrich) dissolved in absolute ethanol. In order to promote the hydrolysis step, the reaction temperature was raised from 298 to 338 K. The resulting sol was stirred overnight and gelation occurred in about 12 h. Then the wet gel, after drying under vacuum, was calcinated in air at 923 K for 8 h. The resulting solid was subjected to two reduction/oxidation cycles, up to 1050 K in H_2 (5%/Ar) and up to 500 K in O_2 (5%/He), in order to stabilize the phases composition [11,12]. A surface area of 28 m^2/g was determined by the BET method. Two platinum catalysts, 0.5 and 1 wt%, respectively, from now on PtCZ5 and PtCZ1, were prepared by impregnation of the ceria–zirconia promoter with a solution of $Pt(acac)_2$ in toluene at 343 K. After drying under vacuum, the solid was calcined at 673 K for 5 h in order to decompose the organic ligand.

2.2. In situ XRD experiments and data analysis

The experimental setup for time-resolved XRD experiments at the GILDA beamline of ESRF [13] consists of an imaging-plate (IP) detector (Fuji, 200 × 400 mm^2) that translates horizontally behind a vertical adjustable Ta slit. A fresh IP surface is therefore continuously exposed to the diffracted X-rays during sample treatments, allowing to collect time-resolved X-ray patterns as narrow vertical strips of the Debye rings on the detector. To carry out the in situ structural investigations on the TWCs [7], the sample was loaded in a quartz capillary, 1 mm internal diameter, supported by an aluminum frame fitted in a goniometer head. The capillary was open on both sides allowing the reaction gases to be input at one end and the products to be conveyed to a quadrupole mass spectrometer (VG 650 London, England) at the other end. To avoid gas flow blocking, the coarser powder fraction, with particles of diameters ranging from 80 to 120 μm, were obtained by meshing. A gas flux heater (Hot-air Blower, Cyberstar, Grenoble, France) with remote temperature control allowed the tuning of the sample temperature in the RT–1223 K range.

The XRD experiments were performed at fixed wavelength ($\lambda = 0.73286$ Å). The data were elaborated by the FIT2D program [14], allowing to extract the XRD patterns from the IP. The structural analyses were carried out by Rietveld refinement using the GSAS package [15]. A α-alumina diffraction standard (NIST Standard Reference Material 676) was used for testing the effective temperature experienced by the sample during the heating runs and to determine the sample-to-detector distance. Furthermore, the investigated samples were mechanically mixed in a 1:1 ratio with the chemically inert α-alumina standard. This procedure allowed to exactly determine the correct 2θ scale in the FIT2D extraction route, by fulfilling the requirement that the reference lattice constant of α-alumina is retrieved. The structural parameters and peak shape of α-alumina, as determined in the calibration runs, were kept fixed in the Rietveld analyses on the samples. Pseudo-Voigt peak profiles were used.

A first set of in situ treatments, denoted with "A", were carried out on a fresh PtCZ1 sample at the temperatures of 473, 553, 593 and 773 K. At these temperatures, three successive isothermal gas treatments were performed:

(a) Initially, the sample was fluxed for 30 min with a 10 vol% O_2/He mixture (5 mL/min) to ensure a good and complete oxidation of the sample. In this step no XRD pattern was collected;
(b) Helium was then fluxed (5 mL/min) for 30 min to ensure a cleaned reaction atmosphere. Only in the last 10 min the X-ray beam shutter was opened and the time-resolved XRD patterns were collected;
(c) Finally, after He switching off, the reductive mixture CO/He (0.1 vol% CO, 5 mL/min) was sent for 30 min, keeping the XRD data collection. Taking into account 10 min of pattern recording in He flux (point b above), the overall XRD measurements lasted therefore 40 min.

After the first treatment loop (a–c) at 473 K, the temperature was raised to 553 K and the loop was repeated. This procedure was iterated also at 593 and 773 K, so that the same sample was subjected to four consecutive redox cycles.

A second set of six redox cycles and XRD measurements, denoted with "B", was performed on a fresh PtCZ1 sample. All the cycles were carried out at 773 K, except for the fifth, that was made at 593 K. Each redox cycle was accomplished in the previously described (a–c) sequence, with the only difference that the CO/He flux

(step c) lasted 50 min and therefore that the length of each XRD data collection was 60 min. According to this procedure, in the last experiment a fresh PtCZ5 catalyst was subjected to two redox cycles at 773 K.

Finally, a fresh sample of metal-free ceria–zirconia promoter was subjected to a redox cycle at 773 K. To improve the velocity of the structural evolution, the same gas mixtures of treatments A and B were fluxed at 20 mL/min. The treatment consisted of: flux of O_2/He for 30 min; flux of He for 30 min and recording of the time-resolved XRD patterns during the last 5 min; flux of CO/He, keeping the XRD recording, for 55 min.

3. Results

An example of the structural analysis carried out on the recorded XRD patterns is provided by the first cycle of sample PtCZ5 in CO/He flux at 773 K. The corresponding time-resolved XRD image is reported in Fig. 1a and in the enlargement of Fig. 1b. At a first glance, broken and continuos lines can be observed: while the continuous lines are relative to the α-alumina diffraction standard, that does not undergo any structural modification except for thermal expansion, the lines belonging to the ceria–zirconia phase present a discontinuity originated from the reduction of Ce(IV) (ionic radius 0.97 Å) to Ce(III) (ionic radius 1.12 Å). The larger ionic radius of Ce(III) involves an increase of the lattice constant and the consequent shift of the diffraction peaks towards lower 2θ values. It is clear, by inspection of Figs. 1a and b, that the reduction of cerium takes place in a step-like mode.

After extraction of the XRD patterns using FIT2D, the Rietveld analysis is carried out allowing for the presence of α-alumina (space group *R*-3*ch*) and of ceria–zirconia (fluorite-like, space group *Fm*-3*m*); lines characteristic of Pt phases, either oxide or metal, were not observed in any of the recorded patterns. In Figs. 2a and b, the calculated and residual patterns are reported, showing the fitting run relative to the strip recorded after 17 min (7 min after the CO/He switching on). At this stage, bulk cerium is still in the (IV) oxidation state. Conversely, the fitting shown in Figs. 3a and b concerns the strip recorded at the 54th minute of experiment, when part of bulk Ce(IV) was reduced to Ce(III). Both the reduced and oxidized patterns were suitably analyzed with the α-alumina phase and one ceria–zirconia component with a well-defined lattice constant.

The most evident feature of Fig. 1 is clearly the abrupt rise of the cubic lattice constant *a* during the reduction of the catalyst in CO/He flow. In Figs. 4a and b, the fitting of a representative XRD pattern recorded during the structural transition (at the 34th minute of the XRD experiment) is drawn. The fitting has been carried out with two cubic ceria–zirconia components: phase 1,

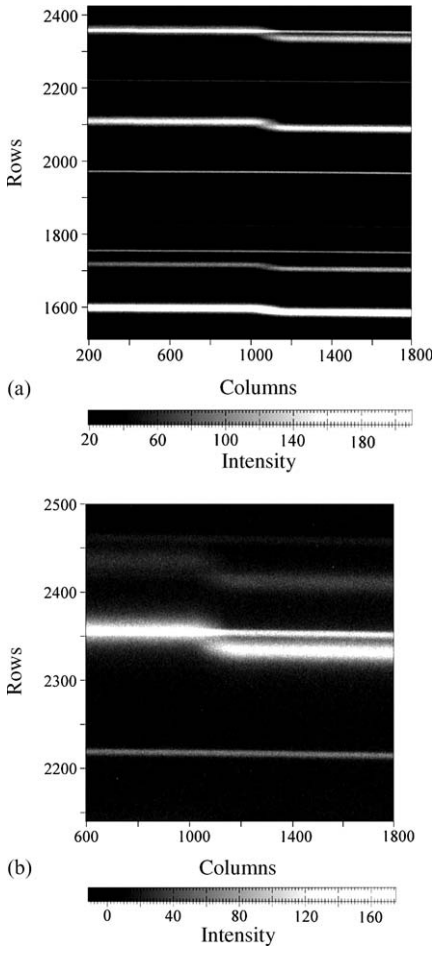

Fig. 1. (a) IP relative to the reduction of the sample PtCZ5 at 773°C. The broken lines are relative to the sudden variation of lattice constant of the ceria–zirconia mixed oxide; the alumina diffraction standard (continuous lines) does not undergo structural modification. (b). Enlargement relative to the (311) ceria–zirconia line, showing in detail the different behavior of ceria–zirconia and of alumina. The gray scales are linear with diffracted intensity. Columns and rows are in units of pixels. The abscissas range (200, 1800) corresponds linearly to the time interval (6 min: 20 s, 56 min: 45 s); the ordinate scale is not linear in 2θ, due to the geometry of the experimental setup. For reference, the strong lines at 1600 and ~2360 are at ~13.5° 2θ and ~26.3° 2θ, respectively.

having a larger amount of Ce(III) ions and, therefore, a larger lattice constant and phase 2, still oxidized in the initial stages of the structural transition. The suitability of introducing two ceria–zirconia components is particularly evident from inspection of Fig. 4b, relative to the high 2θ angles, where the peaks of the two components are well resolved. It cannot be excluded (in fact, fitting runs carried out with three phases gave better agreement between calculated and observed patterns, although with higher correlations between fitting parameters) that even more phases, corresponding to different degrees of reduction, are present. In Fig. 5 the lattice constants of phase 1 and phase 2 are drawn; the phase fraction 1 is

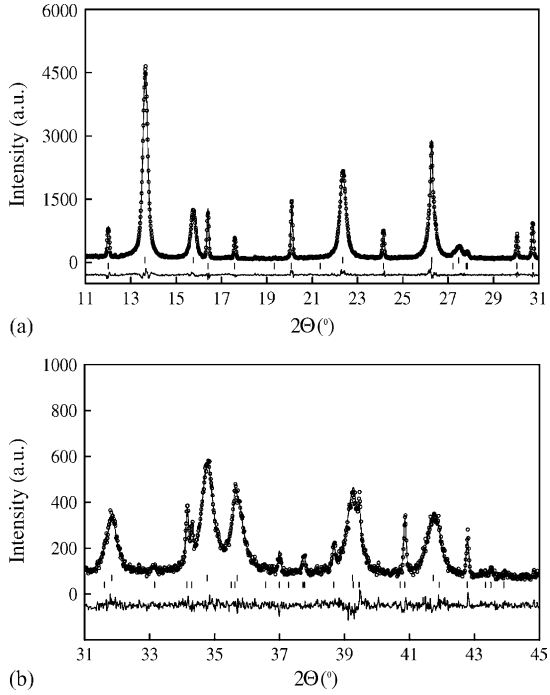

Fig. 2. Experimental data (○) and fitted intensity (—) relative to the still oxidized PtCZ5 sample: (a) in the 11–31° 2θ, (b) the 31–45° 2θ angular interval. Upper tickmarks: ceria–zirconia; lower tickmarks: alumina.

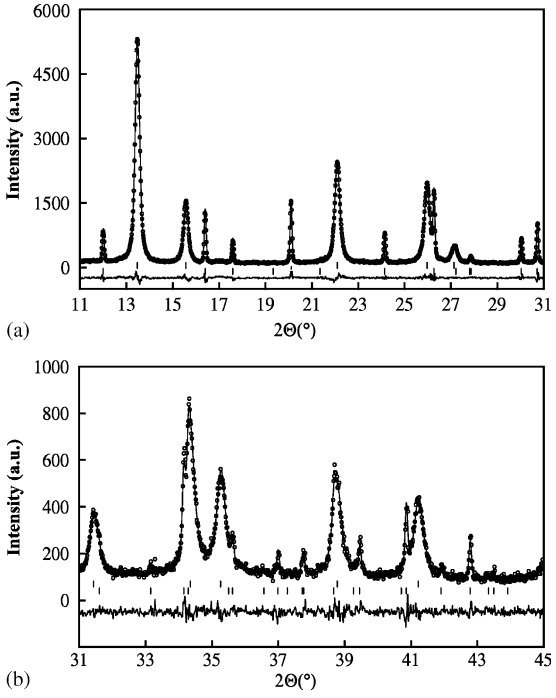

Fig. 3. Experimental data (○) and fitted intensity (—) relative to the reduced PtCZ5 sample: (a) in the 11–31° 2θ, (b) in the 31–45° 2θ angular interval. Upper tickmarks: ceria–zirconia; lower tickmarks: alumina.

also reported, referred to the rightmost ordinate scale. The presence of a still unreacted phase, clearly detectable from 32 min to about 37 min in Fig. 5,

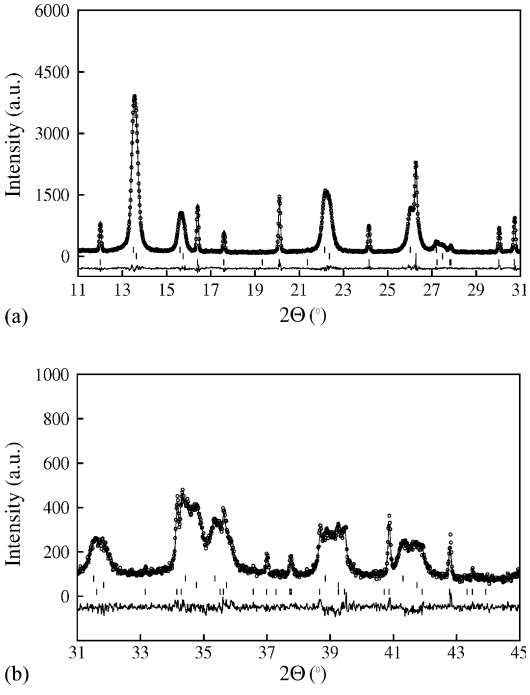

Fig. 4. Experimental data (○) and fitted intensity (—) relative to the PtCZ5 sample during the phase of fast structural variation: (a) in the 11–31° 2θ, (b) in the 31–45° 2θ angular interval. Upper tickmarks: reduced ceria–zirconia; central tickmarks: still-oxidized ceria–zirconia; lower tickmarks: alumina.

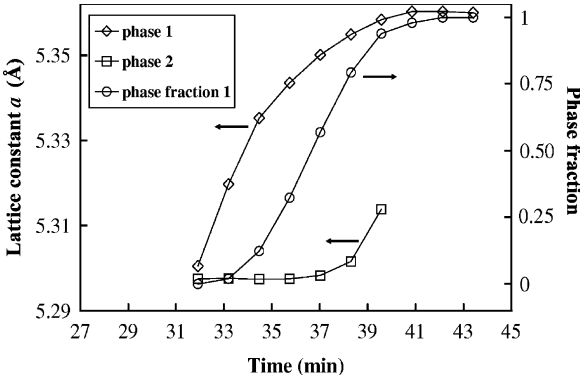

Fig. 5. Lattice constants of the two cubic ceria–zirconia phases detected in the time-resolved XRD pattern of PtCZ5 during structural rearrangement. Phase 1 (◇) is promptly reduced; phase 2 (□) is still oxidized in the 32–37 min time interval and undergoes reduction in the last minutes of the structural transition, while its amount progressively vanishes as the phase fraction 1 (○, right ordinate scale) tends to 1.

indicates that the structural transition takes place at slightly different times for different subvolumes of the sample, while the overall amount of unreacted phase decreases. After an initially fast reduction, each subvolume continues reducing at a slower rate; in the last minutes of the process, from about 37 to 40 min, the reduction of the remaining unreacted fraction is observed. Fig. 6 reports the value of lattice constant of PtCZ5 during the whole period of the in situ XRD

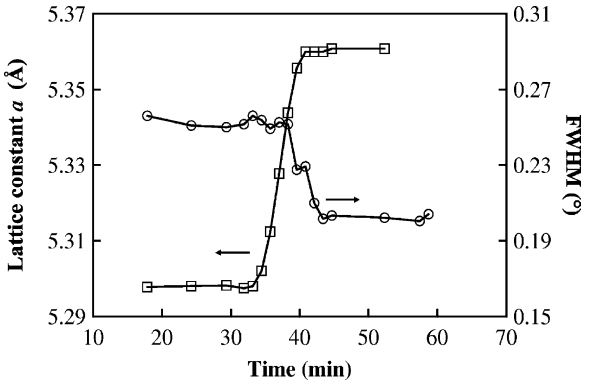

Fig. 6. Average lattice constant of PtCZ5 (□, left ordinate scale) and FWHM of the (220) peak (○, right ordinate scale) during the reduction in CO/He. The errors are of less than 0.01% for lattice constant and of about 5% for FWHM. The CO/He flux is switched on at 10 min, while the structural variation begins at about 35 min, with an induction time of about 25 min.

experiment; the a value during the structural transition is calculated as the mean of the two a values reported in Fig. 5 and weighted with the respective phase amounts. The values of the lattice constants reported in Figs. 5 and 6 are corrected for thermal expansion, assuming that the thermal expansion coefficient is not dependent on the degree of reduction. Before and after the jump, the ceria–zirconia lattice constant does not vary appreciably. This behavior is typical also of the peak width, as can be seen in Fig. 6 (right scale), showing the step-wise decrease of the ceria–zirconia (220) full width at half maximum (FWHM). By reoxidation, the peak width is restored to the initial value; it is likely therefore that the FWHM parameter is associated to an increase of the effective domain size upon reduction, and not to the progressive sintering of the ceria–zirconia particles. As described in the Experimental Section, from $t = 0$ to 10 min the sample is flowed with helium; then, the mixture is switched to CO/He for the successive 50 min. Therefore, the structural rearrangement takes place, for the sample PtCZ5, after an induction time of about 20 min in the exploited reaction conditions of temperature and CO/He gas flow.

The chemical formula of the ceria–zirconia phase, allowing for the partial reduction of cerium, can be written as $Ce(IV)_{1-x-y}Ce(III)_xZr_yO_{2-x/2}$. The stoichiometric coefficients can be calculated under the assumption of linear dependence of the lattice constant on the dopant amount, according to the Vegard's law. This hypothesis found several confirmations in literature on doped ceria [16–18], so that it is likely valid also for the determination of the dopant amount of Zr(IV) and Ce(III). The empirical formula proposed by Kim [18] was used to evaluate as first the amount of zirconium in the fully oxidized sample and then, assuming that the Zr content is independent on the gas flow treatments, the stoichiometric coefficient of Ce(III) [7]. For the fully oxidized PtCZ5 sample, the lattice constant of 5.298 Å, corrected for thermal expansion, was determined. This value fully corresponds to the input preparation amount $y = 0.4$. The composition of the sample after the reduction treatment at 773 K is $Ce(IV)_{0.32}Ce(III)_{0.28}Zr_{0.40}O_{1.86}$.

The structural analysis described for the sample PtCZ5 was carried out for all the in situ XRD data, mainly concerning the PtCZ1 sample, exhibiting a reduction behavior very similar to that of PtCZ5. The catalyst PtCZ1 was subjected to two different redox treatments, described in the Experimental Section as procedures A and B. According to A, a first set of redox treatments was carried out in sequence at the temperatures of 473, 553, 593 and 773 K. The variation of the lattice constant during the reduction with CO/He 0.1 vol% is reported in Fig. 7, showing that the rise is steeper and that the height of the jump is larger at increasing temperatures. Furthermore, an induction time is present at the different temperatures. The behavior of the lattice constant during the B treatment is reported in Fig. 8. It can be observed that the induction time of the subsequent cycles is abbreviated after each subsequent reduction treatment, and that the fifth cycle, although carried out at a lower temperature (593 K), fits well in this trend. On the other hand, the jump of lattice constant is accomplished in nearly the same time for all cycles, no matter of the induction time and of the lower temperature of the fifth cycle. The overall amount of Ce(III) in the fifth cycle is slightly less than at 773 K. Before and after the jump, the cell constant keeps nearly constant, at least on the time scale of the XRD experiment.

The comparison between PtCZ1 and PtCZ5 during the redox cycles at 773 K allowed to see that the a jump is slightly steeper for PtCZ5 and that its induction time

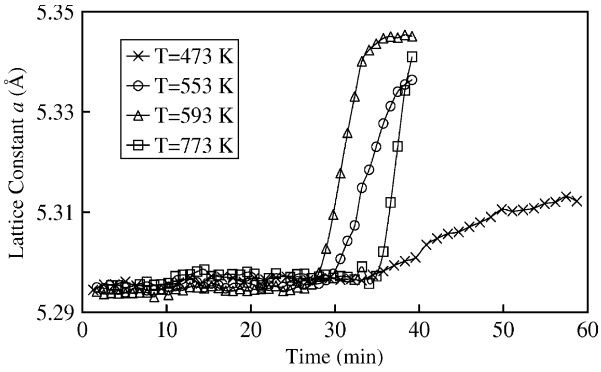

Fig. 7. Variation of the lattice constant of a fresh PtCZ1 sample during successive redox cycles at increasing temperatures. The errors are less than 0.01%. The CO/He flux is switched on at 10 min; the induction time is about the same for the cycles at 553, 593 K while it is longer for the redox cycle at 773 K. The redox cycle at 473 K was repeated on a fresh sample and for a longer period, to get more data about the structural evolution of PtCZ1 at this temperature.

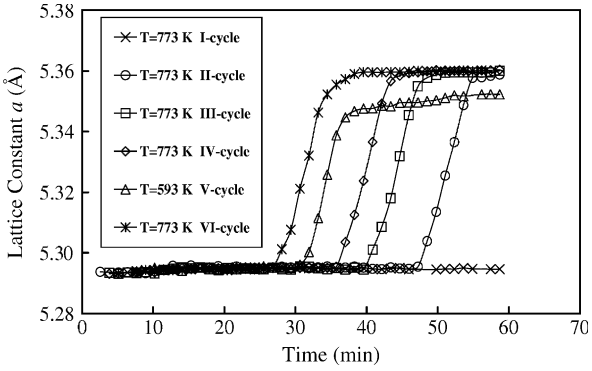

Fig. 8. Variation of the lattice constant of a fresh PtCZ1 sample during successive redox cycles at 773 K (but for the fifth cycle, at 593 K). The errors are less than 0.01%. The CO/He flux is switched on at 10 min; the induction time is larger than 50 min for the first cycle and decreases for the successive cycles. The redox cycle at 593 K fits well this trend.

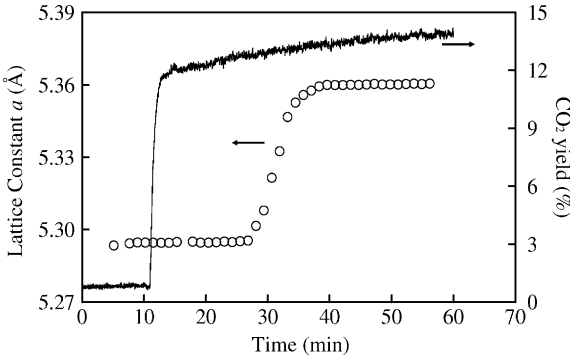

Fig. 9. Comparison between lattice constant (left ordinate scale) and CO_2 production (right scale) for a PtCZ1 sample, showing that the CO_2 production starts with no induction at the CO/He switching on and lasts at a nearly constant (or slightly increasing) rate. The sudden structural rearrangement takes place in the reported case with an induction time of about 20 min. It is possible to observe that the CO_2 yield is not affected at all by the structural rearrangement taking place step-wise at about 30 min.

is shortened in the second redox cycle of PtCZ5, like in the case of PtCZ1. The induction time for the respective fresh samples is definitely shorter for PtCZ5.

During the XRD measurement, the production of CO_2 was monitored by means of mass quadrupole spectroscopy. This part of the experiment allowed to establish that during the flow of CO/He the production of CO_2 is nearly constant, as it is illustrated by Fig. 9, showing also, for comparison, the simultaneous variation of the lattice constant. It is clear that the reduction of Ce(IV) and the CO oxidation proceed in different ways, and in particular that there is not a direct dependence of the degree of bulk reduction of the promoter from the amount of CO_2 detected by mass spectroscopy.

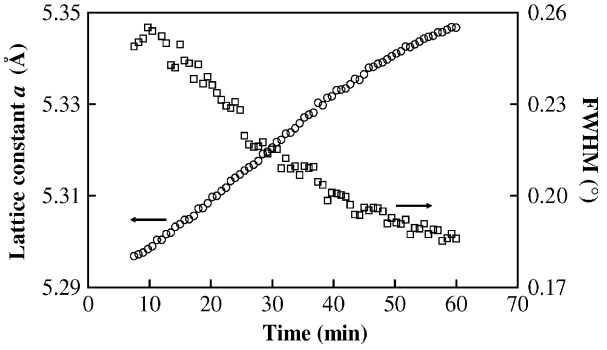

Fig. 10. Lattice constant of unsupported ceria–zirconia (○, left ordinate scale) and FWHM of the (220) peak (□, right ordinate scale) during the reduction in CO/He at 773 K. The CO/He flux is switched on at 5 min. The progressive structural rearrangement in reducing environment is evident.

The reduction behavior of the unsupported ceria–zirconia promoter in CO/He flux is illustrated in Fig. 10, reporting the cell constant and the FWHM of the (220) peak as a function of treatment time. The comparison with Fig. 6 clearly demonstrates that the structural rearrangement in the metal-free promoter takes place in a gradual way.

4. Discussion

The main results of this study can be summarized as follows: (i) the time-resolved XRD patterns show, as a consequence of the reduction processes, a narrowing of the diffraction peaks of ceria–zirconia and their shift towards smaller 2θ angles (Fig. 6); (ii) these phenomena, that take place with an induction time of variable length with respect to the switching on of the CO flux, are carried out in a step-like fashion and are completely reversible through reoxidation of the samples (Figs. 7 and 8); (iii) the production of CO_2 begins immediately after the CO/He flux is sent (Fig. 9), at all the treatment temperatures, and lasts at a nearly constant rate until the catalyst can provide oxygen for the anaerobic oxidation of CO; (iv) the reduction process of unsupported ceria–zirconia (Fig. 10) is completely different from that of Pt/ceria–zirconia (Fig. 6).

The origin of the different reduction mechanisms of the two materials, metal-free and Pt-supported ceria–zirconia, must evidently be ascribed to the presence of the metal phase. It is well established by experimental methods [19] and theoretical analysis [20] that the surface of the supported metal phase constitutes the preferred site of CO adsorption and that CO oxidation is mainly carried out at the metal–support interface with oxygen coming from the support. The observation of an induction time, during which the CO_2 production goes on at nearly constant rate, while the support does not

show evident bulk modification, can be interpreted within this scheme of reaction. According to Martin and Duprez [21], the coefficient for oxygen surface diffusion of ceria is several orders of magnitude larger than the corresponding bulk diffusion parameter, while Giordano et al. [22] found that the step of surface reduction is preliminary to that of bulk reduction in high-surface ($44\,m^2/g$) ceria. On the basis of similar estimates of oxygen mobility, Holmgren and Andersson [23] proposed that oxygen surface diffusion in a Pt/ceria catalyst is a fast process with respect to bulk diffusion. Assuming things in ceria–zirconia not so different from ceria, it seems sound to conclude that the in situ XRD experiments on Pt/ceria–zirconia provided evidence that the first stage of promoter reduction by CO involves the consumption of surface oxygen at the metal–support interface and, considering the nearly constant CO_2 yield, that CO_2 desorption is rate-limiting.

After the induction period, bulk reduction of ceria–zirconia takes place through diffusion of oxygen vacancies into the bulk; this process depends on the temperature and, in particular at 773 K, is very fast on the time scale of CO_2 production. Also, in this phase no sharp variation in the rate of CO_2 can be observed, allowing to conclude that, like during surface reduction, CO_2 desorption continues to be the rate-determining step. The hypothesis that bulk reduction of ceria is a fast process was already made by Martin and Duprez [21] and by Giordano et al. [22]. In particular, the latter authors pointed out that the bulk diffusion length of oxygen at 700 K is about one order of magnitude larger than the typical crystallite size for high-surface ceria, concluding that the oxygen diffusion is not the limiting step for ceria reduction. Holmgren et al. [24] estimated that at 623 K oxygen takes about 20 h to completely diffuse through a 120 Å pure ceria crystallite, but pointed out that this time could be reduced by a factor of 1000 at 673 K, if the oxide was oxygen defective. The different behavior of the metal-free support must be related to the mechanism of CO oxidation, that in this case can be carried out at any site on the exposed surface of ceria–zirconia and involves the gradual consumption of oxygen coming both from the surface and the bulk of the mixed oxide. On the contrary, in Pt-supported ceria–zirconia the CO oxidation proceeds mainly at the metal–support interface and initially involves the more mobile surface oxygens [25]. Although the matter is still object of debate [26,27], a possible explanation of this behavior could be found in the hypothesis proposed for the first time by Frost [28] that the supported metal particles improve the concentration of surface oxygen vacancies of the carrier through a transfer of electronic charge on the metal. So, the higher concentration of oxygen vacancies enhances the surface oxygen mobility towards the interface with the metal and is therefore at the origin of the induction period for bulk reduction.

The other evident structural modification associated with bulk reduction produces the narrowing of the diffraction lines (Fig. 6); also this occurrence is totally reversible under reoxidation and it cannot therefore be ascribed to sintering effects. It could be due to the larger ionic radius of Ce(III) ions, that can partially compensate for the large strain introduced in the structure by the small Zr(IV) ions [29].

The cycles at 473, 553 and 593 K in Fig. 7 show about the same induction time (although the initial rate of a variation at 473 K is so slow that it is hard to precisely define the beginning of bulk reduction), while the delay time at 773 K is enlarged (Fig. 7). This larger induction time with respect to the lower treatment temperatures is found also in the series of reduction–oxidation cycles performed at 773 K (Fig. 8) and could be related to a more effective oxidation. In the successive redox cycles of treatment B (Fig. 8), the induction time progressively decreases from more than 50 min to about 17 min and the fifth cycle at 593 K fits this trend. The data of the in situ XRD experiments suggest that the induction times are function of several parameters such as the amount of supported metal, the treatment temperature and the history of the sample. It is clear that further investigations are necessary to get a fully satisfactory explanation of the metal–support interaction; in particular, X-ray absorption experiments on the Pt L-edges are planned, also to overcome the fact that XRD cannot see the Pt particles. On the basis of the existing evidences, the sources of variable induction times could be, besides the effectiveness of the oxidation step, a progressive modification of the metal–support interaction and/or the enhanced mobility of bulk oxygens.

The modification of the Pt–ceria interaction by reduction treatments has been investigated by several authors in the frame of a strong metal–support interaction. Mullins and Zhang [30] demonstrated that reduction pretreatments modify the strength of CO adsorption on a Pt/ceria catalyst or, if the pretreatment is carried out at temperatures higher than 800 K, that a drastic drop in the adsorption capacity of CO is produced. Bitter et al. [31] used X-ray absorption spectroscopy to demonstrate that reduction pretreatments at 773 K induce a modification of the electronic structure of the supported Pt particles, while only at higher reduction temperatures decoration of Pt by ceria can be observed. Zhou et al. [32] demonstrated by X-ray photoelectron spectroscopy that Pt deposited on a reduced ceria film diffuse in the oxide giving rise to the formation of Pt–Ce bonds. Holmgren et al. [5] found that a mild reduction pretreatment at 473 and 573 K improves the low-temperature catalytic activity of a Pt/ceria catalyst and that this treatment is more effective with a moderate rather than with low Pt dispersion. All these results demonstrate that the interaction of the metal phase with a ceria-based

support is a function of the state of reduction of the catalytic system.

In the course of the anaerobic oxidation of CO performed during the time-resolved XRD experiments at 773 K, it is likely that the metal–support interaction is modified, leading either to an increase of Pt dispersion originated by diffusion of Pt in ceria–zirconia [32] and/or to electronic effects [31]. The degree of metal–support contact affects the catalytic properties [5]. In particular, the longer induction time of fresh PtCZ1 with respect to fresh PtCZ5 could be attributed to a less effective metal–support contact due to lower dispersion of the metal in PtCZ1. It can be also hypothesized that the in situ reoxidation treatments are not sufficient to restore exactly the situation of the metal–support interface of the fresh catalyst, so that the materials keep memory of the previous treatments in the iterated redox cycles and, as a consequence, show a shortening of the induction times.

As mentioned above, the shortening of the induction times could also depend on an improved mobility of bulk oxygens. Mamontov et al. [33] demonstrated by wide-angle neutron scattering that ceria–zirconia presents a notable amount of Frenkel defects, with oxygens that are found in octahedral interstices rather than in the crystallographic tetrahedral sites. These oxygens can hardly be forced in the tetrahedral sites even after prolonged treatment in air at high temperature and are more available for exchange with the reaction environment [33]. It is possible therefore that after each reoxidation step an increasing amount of oxygens do not return in the regular tetrahedral site, remaining in a higher-energy state in the more roomy octahedral sites and producing a net increment of mobile anions in the successive reduction–oxidation cycles. The behavior of metal-free ceria–zirconia seems to support this hypothesis (A. Martorana et al., in preparation).

5. Conclusions

The structural modification of Pt/ceria–zirconia TWC catalysts during the anaerobic oxidation of CO is studied by XRD in situ. The technique allowed to establish that a first stage of the support reduction involves consumption of surface oxygens and that only after an induction time of variable length, the bulk reduction takes place as a fast process. The variable induction time probably depends on the metal–support interaction, leading to a modified metal–support interface and to fine tuning of the electronic properties of the catalyst, and on the presence of an increasing amount of oxygens in the interstitial octahedral sites, more available to exchanges with the reaction environment. Both surface and bulk oxygen diffusion are faster than CO_2 desorption. This conclusion can account for the nearly constant CO_2 production rate during the whole process of ceria–zirconia reduction.

References

[1] A. Trovarelli, Catalysis by ceria and related materials, in: G.J. Hutchings (Series Editor), Catalytic Science Series, Vol. 2, Imperial College Press, 2002.
[2] J. Kaspar, P. Fornasiero, M. Graziani, Catal. Today 50 (1999) 285–298.
[3] R. Burch, J.P. Breen, F.C. Meunier, Appl. Catal. B 39 (2002) 283–303.
[4] Y.J. Mergler, A. van Aalst, J. van Delft, B.E. Nieuwenhuys, Appl. Catal. B 10 (1996) 245–261.
[5] A. Holmgren, F. Azarnoush, E. Fridell, Appl. Catal. B. 22 (1999) 49–61.
[6] G. Centi, P. Fornasiero, M. Graziani, J. Kaspar, F. Vazzana, Top. Catal. 16–17 (2001) 173–180.
[7] A. Martorana, G. Deganello, A. Longo, F. Deganello, L. Liotta, A. Macaluso, G. Pantaleo, A. Balerna, C. Meneghini, S. Mobilio, J. Synchrotron Radiat. 10 (2003) 177–182.
[8] M. Ozawa, M. Kimura, A. Isogai, J. Mater. Sci. 26 (1991) 4818–4822.
[9] J.A. Rodriguez, J.C. Hanson, J.-Y. Kim, G. Liu, A. Iglesias-Juez, M. Fernandez-Garcia, J. Phys. Chem. B 107 (2003) 3535–3543.
[10] R.D. Gonzalez, T. Lopez, R. Gomez, Catal. Today 35 (1997) 293–317.
[11] L.F. Liotta, A. Macaluso, G. Pantaleo, A. Longo, A. Martorana, G. Deganello, G. Marcì, S. Gialanella, J. Sol–Gel Sci. Technol. 26 (2003) 235–240.
[12] L.F. Liotta, A. Macaluso, A. Longo, G. Pantaleo, A. Martorana, G. Deganello, Appl. Catal. A 240 (2003) 295–307.
[13] C. Meneghini, G. Artioli, A. Balerna, A. Gualtieri, P. Norby, S. Mobilio, J. Synchrotron Radiat. 8 (2001) 1162–1166.
[14] A. Hammersley, ESRF Copyright, 1987–2001.
[15] A.C. Larson, R.B. Von Dreele, GSAS, The general structure analysis system, Los Alamos National Laboratory, 1991–2001.
[16] T. Miki, T. Ogawa, M. Haneda, N. Kakuta, A. Ueno, S. Tateishi, S. Matsuura, M. Sato, J. Phys. Chem. 94 (1990) 6464–6467.
[17] S.J. Hong, A.V. Virkar, J. Am. Ceram. Soc. 78 (1995) 433–439.
[18] D.J. Kim, J. Am. Ceram. Soc. 72 (1989) 1415–1421.
[19] T. Bunluesin, H. Cordatos, R.J. Gorte, J. Catal. 157 (1995) 222–226.
[20] V.P. Zhdanov, B. Kasemo, Appl. Surf. Sci. 135 (1998) 297–306.
[21] D. Martin, D. Duprez, J. Phys. Chem. 100 (1996) 9429–9438.
[22] F. Giordano, A. Trovarelli, C. de Leitenburg, M. Giona, J. Catal. 193 (2000) 273–282.
[23] A. Holmgren, B. Andersson, J. Catal. 178 (1998) 14–25.
[24] A. Holmgren, D. Duprez, B. Andersson, J. Catal. 182 (1998) 441–448.
[25] C. Bozo, N. Guilhaume, E. Garbowski, M. Primet, Catal. Today 59 (2000) 33–45.
[26] T. Ioannides, X.E. Verykios, J. Catal. 161 (1996) 560–569.
[27] V.P. Zhdanov, Surf. Sci. 512 (2002) L331–L334.
[28] J.C. Frost, Nature 334 (1988) 577–581.
[29] G. Balducci, J. Kaspar, P. Fornasiero, M. Graziani, M. Saiful Islam, J.D. Gale, J. Phys. Chem. B 101 (1997) 1750–1753.
[30] D.R. Mullins, K.Z. Zhang, Surf. Sci. 513 (2002) 163–173.
[31] J.H. Bitter, M.A. Cauqui, J.M. Gatica, S. Bernal, D.E. Ramaker, C.D. Koningsberger, Stud. Surf. Sci. Catal. 130 (2000) 3183–3188.
[32] Y. Zhou, M. Nakashima, J.M. White, J. Phys. Chem. 92 (1988) 812–818.
[33] E. Mamontov, T. Egami, R. Brezny, M. Koranne, S. Tyagi, J. Phys. Chem. B 104 (2000) 11110–11116.